Long-Distance Magnetic Interaction between a $Mn^{III}Mn^{IV}$ ($S = 1/2$) Core and an Organic Radical: A Spectroscopic Model for the $S_2Y_z^{\bullet}$ State of Photosystem II**

Dana S. Marlin,* Eckhard Bill,*
Thomas Weyhermüller, Eva Rentschler, and
Karl Wieghardt*

The nature of the magnetic interaction between the tyrosine radical $Y_z^{\bullet}$ and the paramagnetic manganese cluster at the reaction center of photosystem II (PSII) has generated a long-standing controversy within the bioinorganic community.[1–3] In PSII, the oxidation of water to molecular oxygen occurs in five discrete steps which have been labeled S_0 through S_4.[4] In the S_2 state, the tetranuclear manganese cluster has an effective spin $S = 1/2$ and exhibits a multiline EPR spectrum that bears resemblance to that from an antiferromagnetic interaction in a $Mn^{III}Mn^{IV}$ dimer.[5–7a] In addition, EPR spectra of the S_2 state feature a second signal at $g = 4.1$ which, under certain conditions, also has an underlying multiline pattern.[7a,b] However, despite extensive studies, the origin of this signal and the induced hyperfine splitting remain unclear.

In PSII samples depleted of Ca^{2+} or Cl^-, the S_2 to S_3 transition is blocked and water oxidation is inhibited.[8] Illumination of these depleted preparations at 273 K results in a state wherein a magnetic interaction between $Y_z^{\bullet}$ and the paramagnetic manganese cluster ($S = 1/2$) is detected. This state is often referred to as $S_2Y_z^{\bullet}$. At the heart of the controversy is the proximity of $Y_z^{\bullet}$ to the manganese cluster in $S_2Y_z^{\bullet}$ as well as the strength and type of coupling between the two spins.[9–14] The significance of the distance is manifested in several proposals for the mechanism of water oxidation that are based on the interplay between these two paramagnets and the possibility of electron transfer between them.[9–15] However, even with the use of powerful magnetic resonance techniques there remains much uncertainty regarding the distance and nature of the interaction between the two $S = 1/2$ centers.[9–14] Proposals for the distance that range from 4.5 Å[16] to 30 Å,[17] and more recently centered around 8 Å,[13,14] attest to the complexity of such an interaction and the difficulties associated with interpretation of spectroscopic data in the absence of concrete model systems.

Indeed, not until the recent monumental crystallographic feat by Zouni et al. and solution of the X-ray structure of PSII (in the S_1 state) at a resolution of 3.8 Å was the location of Y_z verified, and a distance of 7.5 Å measured between Y_z and the Mn cluster.[18] The crystallographic data of the S_1 state, however, only serve to put constraints on the metric parameters between these centers in $S_2Y_z^{\bullet}$, and are not a direct solution to the problem.

Synthetic complexes that model such long-distance Mn_n/organic radical ($n \geq 2$) interactions are lacking in the literature. Such model complexes would not only be useful for detailed analysis of the effect that distance has on the strength of the magnetic coupling, but would also allow a thorough physical description of such interactions wherein dipole coupling may be distinguished from exchange coupling, and subtle rhombicity and Euler angle dependent effects may be observed. Therefore, we have endeavored to synthesize and thoroughly characterize such manganese model complexes wherein weak, long-distance coupling interactions exist, and to provide a detailed description of the electronic structure of these models. Herein we report one such complex, namely $\mathbf{1}(ClO_4)_2$, that possesses a weak interaction between an organic radical ($S = 1/2$) and an antiferromagnetic exchange coupled $Mn^{III}Mn^{IV}$ dimer ($S = 1/2$). A spin-triplet ground state for this complex has been clearly identified, and in addition, the multiline half-field signal (at $g = 4$) that arises from such an interaction, to our knowledge, is shown here for the first time in a dimanganese/organic radical coupled system.

$[(Me_4dtne)Mn^{III}Mn^{IV}(\mu\text{-}O)_2(\mu\text{-}O_2CPhNIT)](ClO_4)_2$ $\mathbf{1}(ClO_4)_2$

Compound $\mathbf{1}(ClO_4)_2$ was synthesized by reacting two equivalents of $Mn(ClO_4)_2$ with Me_4dtne[19] and $HO_2CPhNIT$[20] in acetonitrile. Oxidation of $2\,Mn^{II}$ to $Mn^{III}Mn^{IV}$ was accomplished in air following addition of aqueous NaOH (3 equiv). Addition of excess $NaClO_4$ resulted in separation of microcrystalline $\mathbf{1}(ClO_4)_2$[21] from the reaction mixture. X-ray quality crystals of $\mathbf{1}(ClO_4)_2$[22] were obtained by recrystallization from acetonitrile. A drawing of the structure of dication **1** is displayed in Figure 1a, while selected bond lengths and angles are presented in an expanded view shown in Figure 1b.

Three especially noteworthy characteristics derived from the metric parameters of **1** are as follows: The first is a clear identification of separated Mn^{III} and Mn^{IV} centers illustrated

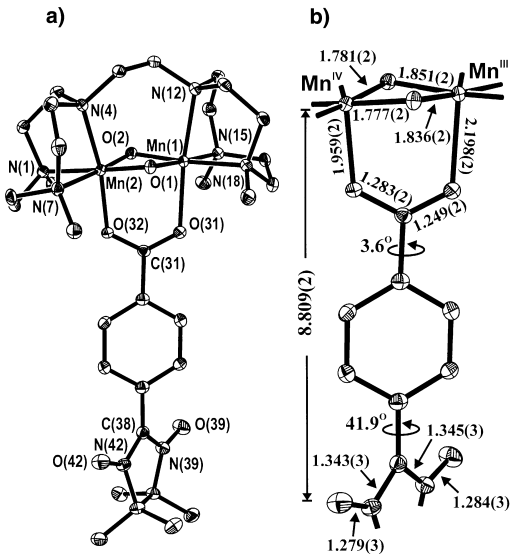

Figure 1. a) X-ray crystal structure of cation **1** (50% thermal ellipsoids). b) Expanded view of a portion of **1** showing selected bond lengths and angles.

[*] Dr. D. S. Marlin, Dr. E. Bill, Prof. Dr. K. Wieghardt,
Dr. T. Weyhermüller, Dr. E. Rentschler
Max-Planck-Institut für Strahlenchemie
Stiftstraße 34-36, 45470 Mülheim an der Ruhr (Germany)
Fax: (+49) 208-306-3952
E-mail: marlin@mpi-muelheim.mpg.de
bill@mpi-muelheim.mpg.de
wieghardt@mpi-muelheim.mpg.de

[**] This work was supported by the Fonds der Chemischen Industrie.

  0044-8249/02/4124-4775 $ 20.00+.50/0

by the difference in bond lengths of the Mn centers to the bridging ligands that form the $Mn^{III}Mn^{IV}$(μ-carboxylato)di(μ-oxo) core. For the Mn^{III} ion these distances are 2.198(2), 1.851(2), and 1.836(2) Å, while for the Mn^{IV} center these bonds contract by approximately 0.1 Å (Figure 1b). The second important characteristic is the equivalence of the two N–O and of the two N–C bond lengths as well as the similar thermal displacement parameters of the nitronyl nitroxide moiety (NIT), indicating that a) the unpaired electron is equivalently present on both O(39) and O(42) atoms of this O-N-C-N-O fragment, and b) no noticeable decomposition of the NIT fragment results from the synthesis.[23] The third characteristic is the asymmetry between the individual Mn centers and the oxygen atoms of the NIT ligand. This results from the different bond lengths in the $Mn^{III}Mn^{IV}$(μ-carboxylato)di(μ-oxo) core noted above, and also the twist of the N(42)-C(38)-N(39) plane of the NIT ligand relative to the O(32)-C(31)-O(31) plane (Figure 1b). Although this latter characteristic is probably a solid-state phenomenon, the asymmetry of the radical relative to the $Mn^{III}Mn^{IV}$ core is also evidenced in solution from EPR spectra of **1** (see below).

The magnetic properties[24] of the three-spin system **1** were explored by multiple-field variable-temperature magnetization measurements on powdered $\mathbf{1}(ClO_4)_2$ (Figure 2). The

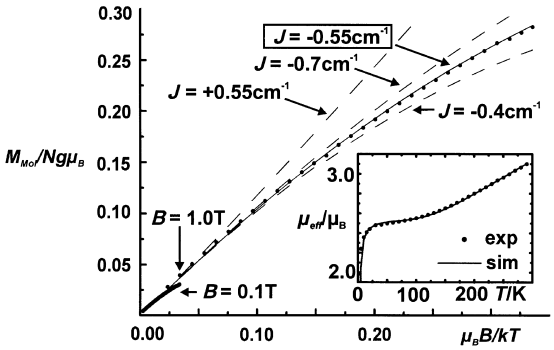

Figure 2. Multiple-field and variable-temperature SQUID magnetic measurements and magnetic moment (inset) measurements on $\mathbf{1}(ClO_4)_2$. Measurement (···) and simulation (——).

overall variation of the magnetic moment of $\mathbf{1}(ClO_4)_2$ with temperature was satisfactorily simulated by using the symmetric spin Hamiltonian [Eq. (1)] with $S_{NIT}=1/2$, $S_{Mn^{III}}=2$, $S_{Mn^{IV}}=3/2$ (Figure 2 inset). Strong antiferromagnetic coupling was found for the manganese ions, $J_{Mn}=-127\ cm^{-1}$, and weak antiferromagnetic coupling for the manganese(III)/organic radical and manganese(IV)/organic radical exchange interaction, $J'=-1(\pm 1)\ cm^{-1}$.

$$H = -2J'\,\mathbf{S}_{NIT}\,(\mathbf{S}_{Mn^{III}}+\mathbf{S}_{Mn^{IV}}) - 2J_{Mn}\,\mathbf{S}_{Mn^{III}}\,\mathbf{S}_{Mn^{IV}} + \sum \mu_B\,\mathbf{S}_i\,\mathbf{g}_i\,\mathbf{B} \qquad (1)$$

Since J_{Mn} is much larger than J' (and $J_{Mn} \gg kT$ at liquid helium temperatures) the spin ground state of **1** can be regarded as a subsystem of two interacting $S=1/2$ species, that is, the radical and the manganese cluster ground state. Correspondingly, the low-temperature behavior ($T<100$ K) of the effective magnetic moment μ_{eff}, closely resembles that of two weakly coupled $S=1/2$ species for which a spin-only value of 2.45 μ_B is expected. Data for **1** level off at about 2.5 μ_B for T between 10–100 K (Figure 2, inset). The rise of μ_{eff} with $T>120$ K indicates increasing population of excited states as shown for similar antiferromagnetic coupled $Mn^{III}Mn^{IV}$ cores.[6] The isoelectronic dimanganese cluster **2** without a NIT pendant arm exhibits strong antiferromagnetic coupling and has an excited spin quartet at $\Delta E = 3J_{Mn} = -360\ cm^{-1}$ above the ground doublet.[6] The radical/cluster interaction renders the ground state of **1** a subsystem of close-lying singlet–triplet states, $|S\rangle$ and $|T\rangle$, with exchange and zero-field splittings (zfs) arising from dipolar and exchange interaction of the NIT radical ($S_{NIT}=1/2$) and the manganese cluster ($S^*=1/2$). The subsystem is properly described by the interaction Hamiltonian [Eq. (2)], where $\boldsymbol{J}_d$ is the matrix of dipolar coupling and J_0 is the exchange coupling constant ($\boldsymbol{I}$ is a unity matrix). The latter leads to a singlet–triplet splitting, $\Delta_{S-T}=2J_0$ (equivalent to J' from Equation (1)). The cluster spin $S^*=1/2$ is a good quantum number for X-band EPR ($h\nu=0.3\ cm^{-1}$) or low-temperature magnetic experiments since the energy gap to other excited total spin manifolds is more than 300 cm^{-1}. The strength of the cluster/NIT exchange interaction was accurately determined from multiple-field magnetization data that were sampled in the range 2–30 K on a $1/T$ scale as shown in Figure 2. A value for J_0 of $-0.55\pm 0.1\ cm^{-1}$ was determined from this model. From single crystal analysis, we presume that this weak exchange coupling arises from *intra-* rather than *intermolecular* coupling. The crystal packing of $\mathbf{1}(ClO_4)_2$ shows that the individual cations of **1** stack in a head-to-tail fashion with the Mn ions sheltered by the Me_4dtne ligands such that there is no close or direct contact between Mn and the NIT oxygen atoms of neighboring molecules. Additionally, the closest intermolecular through-space NIT–NIT distance is approximately 6 Å. Unfortunately, EPR-intensity and Boltzmann depopulation measurements ($1.7\ K<T<15\ K$) designed to probe the singlet–triplet splitting for **1** in frozen solution were obscured by saturation effects even at a low microwave power of 200 nW.

$[(Me_4dtne)Mn^{III}Mn^{IV}(\mu\text{-}O)_2(\mu\text{-}O_2CMe)]^{2+}$ **2**

$$H_{pair} = \mathbf{S}_{NIT}\,(\mathbf{J_d} - 2J_0\,\mathbf{1})\,\mathbf{S}^* \qquad (2)$$

X-band EPR measurements[25] performed on **1** in perpendicular and parallel mode, and also for related complexes **3** and **4** in perpendicular mode are displayed in Figure 3c, d, a and b, respectively.[26] The latter two represent the "parent" species of the spin-pair complex **1**, namely the mixed-valence $Mn^{III}Mn^{IV}$ dimer with its characteristic 16-line pattern (Figure 3a),[6] and the unperturbed NIT signal ($S_{NIT}=1/2$) also with characteristic organic radical hyperfine splittings (Figure 3b).[27] In the latter spectrum the homovalent manganese cluster of **4** is EPR-silent due to strong antiferromagnetic exchange of the Mn^{IV} ions and an effective electron spin $S_{eff}=0$ ground state.[6] The EPR spectrum of **1** in perpendicular mode (Figure 3c) is very different from that of the "parents" due to significant intramolecular interaction described by Equation (2). The dominant feature in the spectrum in Figure 3c is a broad derivative signal at $g=2$

  0044-8249/02/4124-4776 $ 20.00+.50/0 *Angew. Chem. Int. Ed.* **2002**, *41*, No. 24

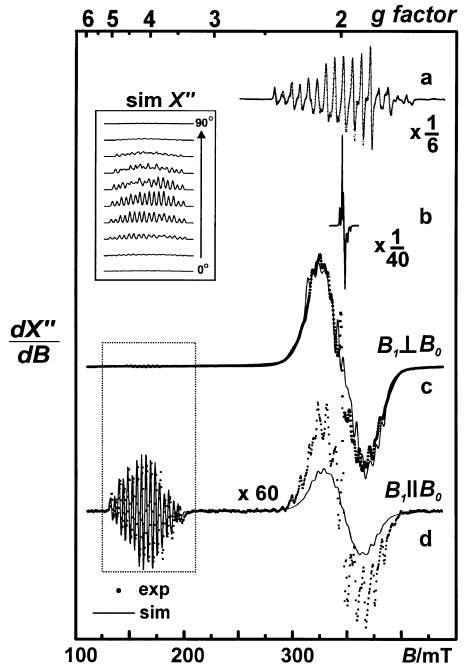

Figure 3. X-band EPR measurements (···) and simulations (——) of **1** (perpendicular (c) and parallel modes (d)), **3** (a) and **4** (d) showing reduction factor of **3** and **4** and magnification of **1** (parallel mode) relative to **1** (perpendicular mode). Experimental conditions for complex: **1**: 1.0 mM CH_3CN glass with 10 mM $tBu_4N{\cdot}PF_6$ at $T = 20$ K and MW power = 636 μW; **3**: 1.0 mM, CH_3CN glass at $T = 30$ K and 200 μW MW power; **4**: 0.1 mM, CH_3CN glass with 10 mM $tBu_4N{\cdot}PF_6$ at $T = 50$ K and 50 μW MW power. Inset shows single-crystal type simulations of the signal at $g = 4$ as a function of θ.

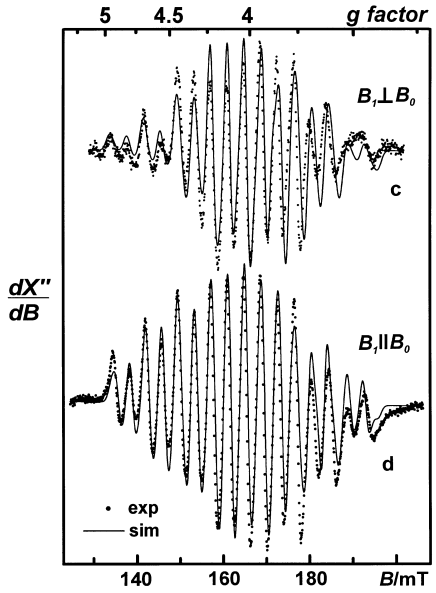

Figure 4. Dual-mode X-band EPR spectra of the $g = 4$ regions for the spectra of **1** shown in Figure 3c (perpendicular mode) and 3d (parallel mode) (boxed area in Figure 3).

featuring less overall splitting than seen for **3** (Figure 3a). However, the most striking aspect of the spectrum of **1** is the presence of a well resolved, multiline signal at $g = 4$ which resembles somewhat the 16-line pattern seen for **3** at $g = 2$. In the parallel mode X-band EPR spectrum of **1** (Figure 3d) the intensity of the "allowed" transitions are greatly attenuated relative to the "forbidden" transitions as a result of the different selection rule $\Delta m = 0$ for $\boldsymbol{B_1} \,||\, \boldsymbol{B_0}$. Figure 4 shows amplified views of the half-field spectra at $g = 4$ of **1** for both perpendicular (Figure 4c) and parallel modes (Figure 4d), wherein the intensity of the transitions clearly indicate significant intramolecular dipolar interaction of the cluster/NIT spin pair.

$[(Me_4dtne)Mn^{III}Mn^{IV}(\mu\text{-}O)_2(\mu\text{-}O_2CPh)]^{2+}$ **3**

$[(Me_4dtne)Mn^{IV}Mn^{IV}(\mu\text{-}O)_2(\mu\text{-}O_2CPhNIT)]^{3+}$ **4**

In our preliminary simulations of the pair spectra of **1** we use an effective spin Hamiltonian for a spin-triplet state [Eq. (3)], where D and E/D parameterize the zfs of the triplet that arise from the anisotropic dipolar part $\boldsymbol{J_d}$ of the J interaction matrix used in Equation (2), and $\boldsymbol{I}$ is the nuclear spin (for Mn^{55}, $I = 5/2$).

$$H = D[S_z^2 - 2/3 + E/D(S_x^2 - S_y^2)] + \mu_B \mathbf{S\,g\,B} + \mathbf{S\,A\,I} \qquad (3)$$

In this approach, singlet–triplet transitions are completely neglected. This approximation is justified by the observation of significant exchange splitting, $\Delta_{S-T} \approx 1\ cm^{-1}$, in solid $\mathbf{1}(ClO_4)_2$. In addition, given that mixing of singlet $|S,0\rangle$ and triplet $|T,0\rangle$ levels by Zeeman and hyperfine interaction may be determined by using terms of the order $\mu_B \Delta g B/(4J_0 + D)$ and $AM_I/2J_0$,[28] we estimate (with $J_0 \approx 0.5\ cm^{-1}$, a maximum $\Delta g = \max(g_{Mn,i} - g_{NIT,j}) \approx 0.01$, and typical A values for **1** of $-100 \times 10^{-4}\ cm^{-1}$) that the singlet–triplet contribution is less than 4%. Therefore, the reasonably good fit of X-band spectra ($\boldsymbol{B}_1 \perp \boldsymbol{B}_0$) substantiate this approach. We emphasize that, in particular, the characteristic "forbidden" transitions at $g = 4$ are not affected by the approximation since they owe their origin to "$\Delta m = 2$" transitions between pure $|T,+1\rangle$ and $|T,-1\rangle$ levels.

A thorough description of the electronic structure of the antiferomagnetically coupled $Mn^{III}Mn^{IV}$ core of the related complex **2** by Schäfer et al. provides an ideal foundation for the present study.[6] In this work, an in-depth magnetic resonance investigation for such complexes is presented, and precise $\boldsymbol{g}$ and ^{55}Mn hyperfine coupling tensors as well as tensor axes related to the molecular structure of the complexes have been deduced. The assigned tensor axes place the z direction perpendicular to the $Mn_2(\mu\text{-}O)_2$ plane, while the x and y axes lay in the direction of the two Mn ions and the two μ-O groups, respectively. Virtually the same parameters are found for **3** from an optimization of the simulation shown in Figure 3a. The simulation parameters found for the NIT radical (Figure 3b) are likewise very close to those of the free organic radical.[27] In our preliminary simulations of the X-band spectra of **1** we chose to neglect Euler rotational effects of the principal axes of local $\boldsymbol{g}$ matrices and $\boldsymbol{J_d}$ for the sake of simplicity.

The actual g values and the components of the ^{55}Mn hyperfine coupling tensors are accurately determined by the pattern of the well-resolved $g = 4$ transitions since these are effectively isolated from the zfs parameters. The inset in Figure 3 shows single-crystal type simulations of those tran-

  0044-8249/02/4124-4777 $ 20.00+.50/0

Table 1. The principal values of the g and Mn^{III} and Mn^{IV} hyperfine tensors (A^{III} and A^{IV} respectively) for complexes **1** and **2**.

Complex	g	A^{III} [$\times 10^{-4}$ cm^{-1}]	A^{IV} [$\times 10^{-4}$ cm^{-1}]	g_{iso}	A^{III}_{iso} [$\times 10^{-4}$ cm^{-1}]	A^{IV}_{iso} [$\times 10^{-4}$ cm^{-1}]	Ref.
	x 2.012	−148.1	62.3				
1	y 2.004	−146.8	80.4	2.001	−130.2	71.9	this
	z 1.986	−95.8	73.1				work
	x 1.996	−159.9	64.0				
2	y 2.001	−142.4	74.3	1.993	−135.1	69.9	6
	z 1.983	−103.0	71.5				

sitions (in absorption mode) as a function of the polar angle θ of the magnetic field with the z axis. Their major intensities arise from orientations intermediate between the principal axes. This demonstrates the sensitivity of the simulations for the different spatial components of the g and A matrices. On the other hand, the shape of the allowed transitions at $g = 2$ depend largely on D and E/D, which contribute to the overall width of the spectrum and its intensity distribution, respectively.

The relative intensity of the *half-field transitions*, however, also depends critically on the zfs of the triplet and hence heavily constrains these parameters, particularly the value of D. Accurate values of g and A^{III} and A^{IV} tensors for **1** are obtained from the simulation of the $g = 4$ transitions (Figure 4). The $g = 2$ region in the parallel mode is more complicated due to 1) the attenuation of the $\Delta m = 1$ transitions, and 2) the influence of $|S\rangle$ and $|T\rangle$ mixing. Therefore, a more accurate measure of zfs was obtained from simulation of the $g = 2$ region in perpendicular mode (Figure 3c). The g and A^{III} and A^{IV} tensors for **1** and **2** are listed in Table 1. Deviations between g values obtained here and those reported for **2** are small.[6] Values of $D = -90 \times 10^{-4}$ cm^{-1} and $E/D = 0.30$ were obtained for the zfs of **1**.

Since D owes its origin to the dipole interaction between the radical and manganese cluster, its value is a measure of the "mean" separation of the two spin density distributions given by $D = -3/2\, g^2 \mu_B^2 r^{-3}$ for $E/D = 1/3$ (where $\mu_B^2 = 0.433$ for D in cm^{-1} and r in Å).[29a–c] The value for D of -90×10^{-4} cm^{-1} obtained by simulation yields a corresponding distance between the radical and the cluster of 6.6 Å. The deviation of this value from the shortest molecular distance between the NIT radical and Mn center (8.809(2) Å) is astonishing, especially in the view of application of EPR spectroscopy to gauge distances in other unknown molecules.[12–14,16,17] We attribute the difference to delocalization of spin density and the r^{-3} dependence of the interaction which weight the edges of the respective magnetic orbitals rather than their centers. The average distance from the N–O groups of the NIT moiety to the O atoms of the carboxylate bridge is 7.0 Å and thus noteworthy in this context as it approximates the calculated coupling distance better.

It is important to consider the significance of a large rhombicity parameter, $E/D \approx 0.3$, as simulations with small E/D values for the triplet spectra do not show the appropriate central intensity maxima at $g = 2$.[28] Point-dipoles are unable to induce rhombic zfs of the triplet state due to the intrinsic symmetry between two points. From preliminary dipole-dipole simulations based on Equation (2) with axial ($J_d - 2J_0 \mathbf{1}$) matrix (not shown) we discard Euler rotations of the dipolar arrangement as an alternative explanation of the experimental feature, as it is not equivalent to a rhombic J matrix. Therefore, we attribute the observed rhombicity to the extended nonaxial spatial distribution of the respective spin density on the radical as well as on the manganese cluster moiety.

In conclusion, we have shown that in a relatively simple model for long-distance dimanganese/organic radical exchange interactions, an excellent tool for understanding similar interactions in more complicated systems is found. We demonstrate the efficacy of dual-mode EPR spectroscopy as an additional tool for determining the extent of these long-distance dipolar coupling interactions. We also note that our "simple" system has several complicating features such as asymmetry in the coupling interaction as well as possible contributions to the EPR spectra from singlet–triplet transitions, which have not been addressed here. These more rigorous studies are currently underway in our laboratory with this and related molecular model systems. We also seek to uncover whether there exists a relationship or parallel between our half-field signal at $g = 4$ (with its multiline pattern) and that observed in the S_2 state of PSII.[7a,b]

Received: September 19, 2002 [Z50202]

[1] A.-F. Miller, G. W. Brudwig, *Biochim. Biophys. Acta* **1991**, *1056*, 1.
[2] J. Stubbe, W. A. van der Donk, *Chem. Rev.* **1998**, *98*, 705.
[3] V. K. Yachandra, K. Sauer, M. P. Klein, *Chem. Rev.* **1996**, *96*, 2927.
[4] B. Kok, B. Forbush, M. McGloin, *Photochem. Photobiol.* **1970**, *11*, 457.
[5] G. C. Dismukes, Y. Siderer, *Proc. Natl. Acad. Sci. USA* **1981**, *78*, 274.
[6] K.-O. Schäfer, R. Bittl, W. Zweygart, F. Lendzian, G. Haselhorst, T. Weyhermüller, K. Wieghardt, W. Lubitz, *J. Am. Chem. Soc.***1998**, *120*, 13104.
[7] a) J. M. Peloquin, K. A. Campbell, D. W. Randall, M. A. Evanchik, V. L. Pecoraro, W. H. Armstrong, R. D. Britt, *J. Am. Chem. Soc.* **2000**, *122*, 10926; b) D. H. Kim, R. D. Britt, M. P. Klein, K. Sauer, *J. Am. Chem. Soc.* **1990**, *112*, 9389.
[8] R. J. Debus, *Biochim. Biophys. Acta* **1992**, *1102*, 269.
[9] P. Dorlet, A. Bossac, W. Rutherford, S. Un, *J. Phys. Chem. B* **1998**, *102*, 10945.
[10] V. A. Szalai, H. Kühne, K. V. Lakshmi, G. W. Brudvig, *Biochemistry* **1998**, *37*, 13594.
[11] W. Lubitz, F. Lendzian, R. Bittl, *Acc. Chem. Res.* **2002**, *35*, 313.
[12] M. L. Gilchrist, Jr., J. A. Ball, D. W. Randall, R. D. Britt, *Proc. Natl. Acad. Sci. USA* **1995**, *92*, 9545.
[13] P. Dorlet, M. Di Valentin, G. T. Babcock, J. L. McCracken, *J. Phys. Chem. B* **1998**, *102*, 8239.
[14] K. V. Lakshmi, S. S. Eaton, G. R. Eaton, G. W. Brudvig, *Biochemistry* **1999**, *38*, 12758.
[15] C. W. Hoganson, G. T. Babcock, *Science* **1997**, *277*, 1953.
[16] X.-S. Tang, D. W. Randall, D. A. Force, B. A. Diner, R. D. Britt, *J. Am. Chem. Soc.* **1996**, *118*, 7638.
[17] Y. Kodera, S. A. Dzuba, H. Hara, A. Kawamori, *Biochim. Biophys. Acta* **1994**, *1186*, 91.

  0044-8249/02/4124-4778 $ 20.00+.50/0

[18] A. Zouni, H.-T. Witt, J. Kern, P. Fromme, N. Krauß, W. Saenger, P. Orth, *Nature* **2001**, *409*, 739.
[19] Me_4dtne = 1,2-bis(4,7-dimethyl-1,4,7-triazacyclonon-1-yl)ethane was synthesized according to reference [6].
[20] HO_2CPhNIT = 2-(4-carboxyphenyl)-4,4,5,5-tetramethyl-3-oxyimidazolidin-1-oxide was prepared according to: C. Bätz, P. Amann, H.-J. Deiseroth, L. Dulog, *Liebigs Ann. Chem.* **1994**, 739.
[21] Selected IR stretching frequencies: $\tilde{\nu} = 1584$(m), 1543(m), 1455(m), 1375(s), 1105(s, ClO_4^-), 780(m), 689(m), 624 cm^{-1} (m). EI mass spectra show two molecular ion peaks at m/z 379 for $[\mathbf{1}]^{2+}$ and 857 for $[\mathbf{1}(ClO_4)]^+$. Elemental analyses (%) calcd for $C_{32}H_{56}Cl_2Mn_2N_8O_{14}$: C 40.13, H 5.86, N 11.71; found: C 38.80, H 5.77, N 11.71.
[22] Crystal structure analysis data for $\mathbf{1}(ClO_4)_2$: $C_{32}H_{56}Cl_2Mn_2N_8O_{14}$, $M_r = 957.63$, monoclinic, $P2_1/c$, $a = 11.6313(4)$, $b = 21.4815(10)$, $c = 16.9454(6)$ Å, $\beta = 108.17(1)°$, $V = 4022.8(3)$ Å^3, $Z = 4$, $\rho_{calcd} = 1.581$ Mg m^{-3}, $\mu(Mo_{K\alpha}) = 0.836$ mm^{-1}, $F(000) = 2000$; 56074 reflections collected at 100(2) K; 9213 independent reflections; GOF = 1.079; $R = 0.0448$, $wR2 = 0.0827$. CCDC-192780 contains the supplementary crystallographic data for this paper. These data can be obtained free of charge via www.ccdc.cam.ac.uk/conts/retrieving.html (or from the Cambridge Crystallographic Data Centre, 12, Union Road, Cambridge CB2 1EZ, UK; fax: (+44) 1223-336-033; or deposit @ccdc.cam.ac.uk).
[23] Early synthetic attempts at **1** and variants under less mild conditions resulted in complexes wherein decomposition of the NIT moiety took place yielding the imidazolidin-1-oxide radical product, which was evident from inequivalent thermal parameters of O(42) and O(39).
[24] Magnetization of solid $\mathbf{1}(ClO_4)_2$ was measured by using a SQUID magnetometer (MPMS-7, Quantum Design). The molar susceptibilities were corrected for underlying diamagnetism by using tabulated Pascal constants ($X_{dia} = -400 \times 10^{-6}$ cm^3 mol^{-1}). The routine JULIUS was used for spin Hamiltonian simulations of the data (C. Krebs, E. Bill, F. Birkelbach, V. Staemmler, unpublished results).
[25] EPR spectra were measured for solutions of **1**–**3** in acetonitrile with a Bruker ELEXSYS E300 spectrometer with standard or dual-mode cavity and Oxford Instruments ESR910 flow cryostat. Spin-Hamiltonian simulations were performed with the XSOPHE program by G. Hanson et al. that is distributed by Bruker Biospin GmbH.
[26] The latter two complexes are components of an extended and detailed investigation that will be reported in the future. We include only their X-band EPR spectra here for clarity. For **1** in acetonitrile a small degree of dissociation of the bridging carboxylato ligand O_2CPhNIT$^-$ from the mother complex $[(Me_4dtne)Mn_2(\mu\text{-}O)_2]^{3+}$ is observed. The "impurity" spectra are similar to those in Figure 3a and b and may be easily subtracted from that of intact **1** (shown in Figure 3c). The amount subtracted, integrated to less than 1% by area.
[27] E. Ullman, J. H. Osiecki, D. G. B. Boocock, R. Darcy, *J. Am. Chem. Soc.* **1972**, *94*, 7049.
[28] a) J. E. Wertz, J. R. Bolton, *Electron Spin Resonance*, McGraw-Hill, New York, **1972**; b) P. J. Hore in *Advanced EPR: Applications in Biology and Biochemistry* (Ed.: A. J. Hoff), Elsevier, Amsterdam, **1977**, pp. 405–440.
[29] a) N. M. Atherton, C. J. Winscom, *Inorg. Chem.* **1973**, *12*, 383; b) T. D. Smith, J. R. Pilbrow, *Coord. Chem. Rev.* **1974**, *13*, 173; c) A. Bencini, D. Gatteschi, *EPR of Exchange Coupled Systems*, Springer, Berlin, **1990**.

Real-Time Single-Molecule Imaging of the Formation and Dynamics of Coordination Compounds

Nian Lin,* Alexandre Dmitriev, Jens Weckesser, Johannes V. Barth,* and Klaus Kern*

A current challenge in the field of self-assembled supramolecular nanostructures is the development of strategies for the deliberate positioning of functional molecular species on suitable substrates; this is a crucial aspect in the search for molecular devices.[1] Recent studies revealed that design principles from supramolecular chemistry can be adapted to fabricate unique supramolecular aggregates at surfaces.[2,3] However, to date, mainly hydrogen bonding and electrostatic intermolecular coupling have been successfully exploited to control the ordering of molecular building blocks at low temperatures. These interactions bear the disadvantage of low thermal and mechanical stability. Thus, there is a demand to explore the construction of more rigid supramolecular architectures[4,5] on surfaces. Metal–ligand interactions, which were introduced by Werner at the turn of the 20th century,[6] are recognized as being decisive in molecular recognition and an excellent means for the fabrication of three-dimensional supramolecular arrangements.[7–9] However, the current understanding of the evolution and dynamics of such interactions on surfaces is limited, although their energetics are in a range which lets us expect reaction rates that would permit their direct elucidation at ambient temperature by imaging methods.

For the present investigation conducted on an atomically clean surface we took advantage of ligand systems based on carboxylic acids and transition metals whose characteristics are well understood.[10] Specifically, we addressed metal–ligand bonding of trimesic acid (tma) and Cu atoms. Trimesic acid is a polyfunctional carboxylic acid with threefold symmetry comprised of a phenyl ring and three identical carboxy end groups in the same plane.[11] Its complexation was observed on Cu(100) in ultrahigh vacuum at temperatures in the range 250–300 K following deposition at room temperature. Under these conditions, the carboxylic acid groups are completely deprotonated such that three reactive COO^- ligands per tma molecule exist.[12,13] The deprotonation is presumably related to the availability of Cu adatoms at the surface, which are known to exist on Cu(100) in the employed temperature range. The reason behind the presence of Cu adatoms is their continuous evaporation from atomic step

[*] N. Lin, K. Kern, A. Dmitriev, J. Weckesser
Max-Planck-Institut für Festkörperforschung
Heisenbergstrasse 1, 70569 Stuttgart (Germany)
Fax: (+49) 711–689–1662
E-mail: n.lin@fkf.mpg.de
k.kern@fkf.mpg.de
J. V. Barth, K. Kern
Institut de Physique des Nanostructures
Ecole Polytechnique Fédérale de Lausanne
1015 Lausanne (Switzerland)
E-mail: Johannes.Barth@epfl.ch

Supporting information for this article is available on the WWW under http://www.angewandte.org or from the author.

  0044-8249/02/4124-4779 $ 20.00+.50/0